ACS OMEGA

Open Access

http://pubs.acs.org/journal/acsodf

Article

Output Performance Enhanced Triboelectric Nanogenerators Induced by Magnetic Ink Trapping Property Act as Wearable Sensors

Jingzhe Sun,[§] Jiwoo Lee,[§] Seunghye Han, Yongwei Li, Jong-Jin Park,* and Jihyun Bae*

Cite This: *ACS Omega* 2024, 9, 3565−3573

Read Online

ACCESS | Metrics & More | Article Recommendations | Supporting Information

ABSTRACT: The demand for clean-energy collection has gradually increased in recent years, making triboelectric nanogenerators a promising research field, because of their advantages in convenient manufacturing, diversified materials, and diverse synthesis and modification possibilities. However, recent studies indicate that charge decay, a major limiting factor in the triboelectric output, prevents the induced charge from combining with the bottom electrode, leading to charge loss. The use of charge-trapping sites to retain the induced charge generated during the friction process is an important solution in the field of triboelectric nanogenerator research. This study proposes the use of an elastic ink with macroscopic magnetism as trapping sites by coating the ink as dots between the polytetrafluoroethylene (PTFE) dielectric layer and the electrode layer. Nickel particles in the magnetic ink are doped into the system as microcapacitors, which prevent the combination of the friction layer and induced charges on the back electrode. Because the nickel itself can be used as a charge-potential trap to capture the charge introduced by the charge-injection process, the charge can be maintained for a long time and achieve a long-term high-output state. The output voltage was more than 6 times that of the reference group without the magnetic-ink coating after 3 h. The results provide a reference direction for research on preventing charge decay and trapping charges in triboelectric nanogenerators.

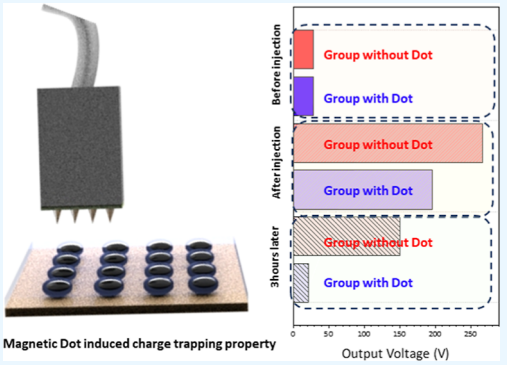

INTRODUCTION

Owing to the increasingly significant greenhouse effect and various environmental problems caused by traditional fossil-fuel energy sources, the collection of clean energy has received increasing attention.[1−3] As a solution for clean energy, triboelectricity has gradually become a promising research field for converting electricity using the charged electrostatic-induction coupling effect. Owing to their simple structure, flexible and diverse materials, and low cost, triboelectric nanogenerators (TENG) are widely used in biosensing, artificial intelligence, and power supply for small equipment.[4,5] The surface-charge density is positively correlated with the output of a TENG and the charge decay induced by the combination process directly leads to a lower output efficiency, thereby limiting its application.[6] To improve the charge density, recent studies have proposed doping particles with a high dielectric constant, increasing the frictional contact area, and charge injection.[7−10] Charge injection can significantly increase the charge density in a short time; however, the injected charge is still lost by being combined with the charge of the back electrode.[11] The charge injected onto the surface is naturally lost to the air because of the lack of trapping sites.[12] Previous studies have maintained charge by increasing the number of trapping sites through chemical modification, adding complex internal structures to increase the trapping area, and doping particles with trapping properties in the friction layer.[13,14] The printing process and the all-printed TENG have also been developed to improve the output performance.[15] However, these methods involve complex manufacturing processes. Thus, developing methods to easily and quickly enhance the trapping properties of TENGs is necessary to maintain a high output performance for a long time.

The introduction of magnetic substances such as nickel into the manufacturing process of the friction layer of TENGs has been reported in the literature,[16,17] while the hysteretic behavior of contact force response in triboelectric nanogenerator has been reported as an earliest related study.[18] However, the previous magnetic body was used as a macroauxiliary body to drive the TENG to complete its friction motion. Alternatively, it could be regarded as a large capacitor with multiple microcapacitors combined in parallel and series when the magnetic-metal material is introduced into

Received: September 27, 2023
Revised: December 22, 2023
Accepted: December 29, 2023
Published: January 10, 2024

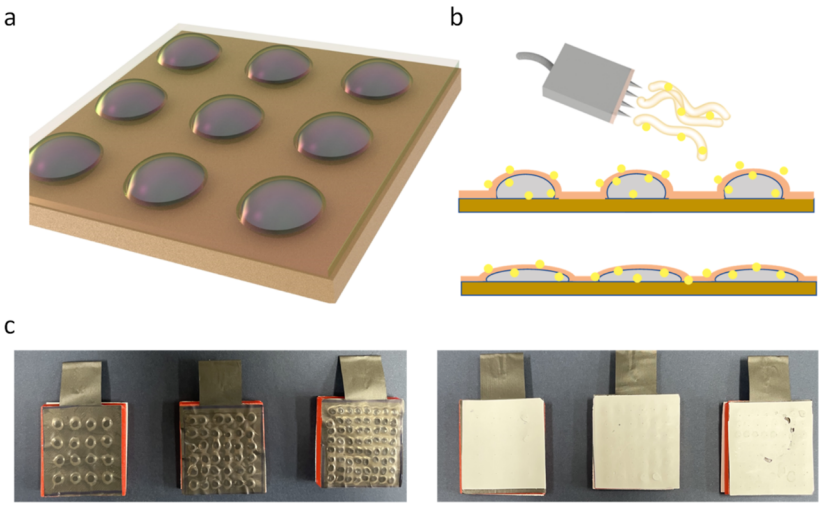

Figure 1. (a) Schematic of the structure of PTFE−magnetic droplets−electrode. (b) Schematic of the charge injection process and the trapping effect of magnetic droplets. (c) Photograph of the PTFE−magnetic dot−electrode and nylon−magnetic dot−electrode.

the friction layer in the form of fine particles using its own high capacitance. This enhances the capacitance of the TENG, thereby increasing the maximum charge it can hold and improving the output performance.[19] No previous reports have investigated magnetic substances as charge-trapping sites and their insertion between the friction layer and the electrode as a trapping layer. Thus, developing a simple magnetic-trapping layer for TENG devices is necessary. The introduction of the trapping properties of the TENG device should be researched by adding a magnetic substance to maintain a high equilibrium surface charge for a long time.

In this study, magnetic ink was used as the trapping site, and the simple method of adding a trapping layer between the friction layer and the electrode was developed to maintain a high-output state for a long time. Elastomer ink droplets containing magnetic nickel were coated on the back of the dielectric layer of polytetrafluoroethylene (PTFE) and nylon films. After drying, half spheres (approximately 0.5 × 0.5 mm) were formed, which served as trapping sites for preserving the surface charge introduced by the charge-injection process. The number of spheres was 4 × 4, 6 × 6, and 8 × 8. Four structures—nylon−PTFE (N-P) (reference group), nylon and magnetic particle−PTFE (NM-P), nylon−PTFE and magnetic particle (N-PM), and nylon, magnetic particle−PTFE and magnetic particle (NM-PM)—were measured to investigate the differences in the trapping properties of positive/negative materials. After the charge-injection process, the N-PM group showed the highest output voltage and trapping properties compared with the basic control group, N-P. Even after 3 h, it maintained 58% of the output voltage after injection, indicating good trapping performance. Finally, the TENG was used as a general sensor to detect human-movement behavior, which demonstrated the application significance of the display. In this study, a simple and fast method is proposed to enhance the properties of TENGs, which provides a feasible reference for the development of TENG devices that maintain high-performance output for a long time.

EXPERIMENTAL SECTION

Materials. PTFE tape (thickness 0.08 t) was purchased from Nitto (Japan). Nylon-11 was purchased from ARKEMA (South Korea). Formic acid (99%) and dichloromethane were purchased from Daejung (South Korea). Magnetic elastomer ink (lot no. 220608-HUNIV) was purchased from Magron (South Korea) (the size of magnetic particles is about 3.5−6 μm, as shown in Figure S1). The conductive fabric used as the electrode (with a back adhesive layer) was purchased from A-jin Electro Company.

Nylon Film Casting Process. First, a mixture of nylon-11 pellets (3 g), formic acid (13.5 g), and dichloromethane (13.5 g) was stirred at 400 rpm and 25 °C in a 100 mL beaker for 2 h to completely dissolve the nylon-11 pellets. The film was obtained by pouring the mixture onto a glass plate and pushing it with a doctor blade set to 100 μm. The film was then dried in an oven at 60 °C for 4 h.

Magnetic Ink Droplets Casting Process. Magnetic ink droplets were placed on the back of the dielectric layer with an eyedropper, heated in an oven at 60 °C for 12 h, and completely dried. After drying, all of the solvent contained in the ink evaporates, and the polymer elastomer acts as a binder to firmly wrap the magnetic particles and fix them on the back of the dielectric layer.

Assemble of TENG Device. The nylon-11 film gained from the casting process is cut to 4 × 4 cm^2, and the PTFE tape is also cut to 4 × 4 cm^2. The textile electrode is attached to the dielectric layer with the back adhesive layer.

Charge Injection Process. Charge injection was performed using a high voltage injection device (Chargemaster VCMBP30) with an output voltage range of −30 to +30 kV, the distance of the needle of the injection device and the film is about 1 cm, and injection time is fixed at 3 min.

Characterization and Measurement. The compression pressure was measured using a push−pull gauge (RZ-50, ALKOH, Japan), and the frequency was tested while controlling the speed of the periodic repetitive motion of a self-made compressing/releasing machine that was used in previous studies. The external force at this time was 20 N, and a frequency of 2.5 Hz was measured. Open-circuit voltages were measured using a digital phosphor oscilloscope (DPO2012B) with an internal resistance of 1 MΩ.

RESULTS AND DISCUSSION

Nylon11, obtained by the casting method, was used as the positive triboelectric material, and commercially available

https://doi.org/10.1021/acsomega.3c07460
ACS Omega 2024, 9, 3565−3573

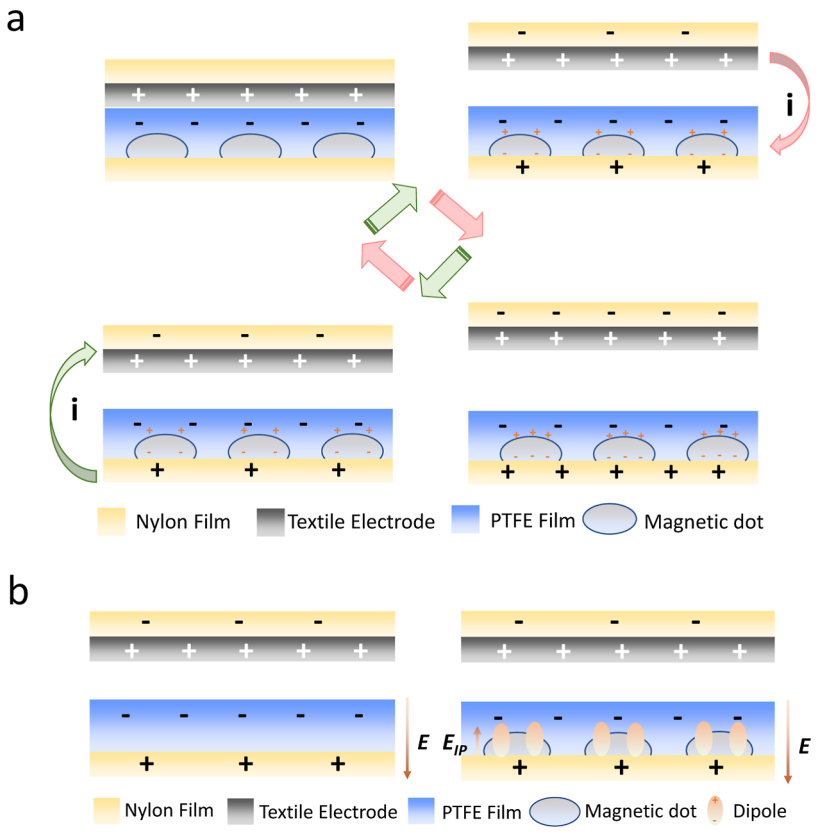

Figure 2. (a) Working mechanism of the magnetic particle contained TENG. (b) Trapping mechanism of the trapping effect induced by the magnetic particles.

PTFE tape was used as the negative triboelectric material to assemble the TENG. Magnetic ink purchased from the MAGRON company was directly deposited on the surfaces of the nylon and PTFE films using a dropper. The dropped viscoelastic polymer ink contained metallic nickel particles. As a viscoelastic polymer falls naturally under gravity, flat droplets form on the film surface. After the polymer was dried at high temperatures, the fabricated electrodes were affixed to the back of the film and assembled. First, a variable design was used for the number of magnetic droplets as follows: 4 (horizontal) × 4 (vertical), 6 × 6, and 8 × 8 dots. This was used to determine the influence of the number of magnets on the output voltage and trapping performance after charge injection (as shown in Figures S2 and S3, the pictures of the push−pull gauge and injection device are attached).

To investigate the difference in the trapping properties of the positive and negative materials after the addition of magnetic particles, the output voltages of the N-P, NM-P, N-PM, and NM-PM structures were measured.

An overview of the experiment is shown in Figure 1 (Figure 1c was taken by one of the authors). Figure 1a shows a conceptual diagram of the TENG structure, where the magnet wrapped with a viscoelastic polymer forms a flat droplet shape. This caused a certain height difference to the surface of the friction layer, which can be regarded as an increase in roughness.[18] In the charge-injection process shown in Figure 1b, a high voltage was applied to the tip of a needle and a strong electric field was generated when the back electrode was grounded. The molecules in the air are ionized, which acquire positive or negative charges and move toward the film.[20] The charged ions were trapped on the surface of the film, significantly increasing the surface-charge density of the friction layer.[21] Owing to the properties of the magnetic polymer elastomer itself, it compressed to a certain extent under pressure; thus, the contact area increased when certain magnetic particles are added. However, if the magnetic particle droplets are over the certain amount, the air will fill the space between the friction layer and the electrode on the back, reducing the overall dielectric constant and capacitance level, also, because of the thickness of the droplets themselves, when the number of droplets increases, leading to an overall thicker structure, eq 1 shows that the surface charge density gradually decreases.[22] Figure 1c shows a photograph of the TENG structure. The left side shows PTFE coated with magnetic droplets, and the right side shows a nylon film coated with magnetic droplets. Nylon is relatively brittle; thus, after the back is coated with liquid droplets, damage inevitably occurs during friction, which also affects the output performance.

$$\sigma = \frac{\varepsilon_0 \varepsilon_r V_{tri}}{d} \tag{1}$$

where σ is the surface charge density, ε_0 is the vacuum dielectric constant, ε_r is the relative dielectric constant of the friction layer, V_{tri} is the triboelectric voltage, and d is the thickness of the dielectric layer.

The operating mechanism of the TENG is illustrated in Figure 2a. The frictional charge generated by a TENG is typically attributed to coupled triboelectrification and electrostatic-induction effects. When the nylon and PTFE films were in full contact with each other, the charge on the nylon surface moved to the PTFE because its Fermi level was considerably higher than that of the PTFE. This resulted in a negative

https://doi.org/10.1021/acsomega.3c07460
ACS Omega 2024, 9, 3565−3573

charge on the PTFE and a positive charge on the nylon surface. When the two friction layers were separated to produce an interval, the back electrode produced opposite charges induced by the charge on the friction layer owing to the electrostatic-induction effect. Electrons flowed from the PTFE-side electrode to the nylon-side electrode, which provided a negative charge, whereas the PTFE back electrode provided a positive charge. When the charge reached equilibrium, PTFE and nylon were completely separated. When pressure was applied again to bring the nylon and PTFE into contact, a reverse current flowed from the PTFE-side electrode to the nylon-side electrode. When the TENG contacts separated, the device alternately generated current owing to the coupling of the contact-charged cation and electrostatic induction.[23] Figure 2b shows a schematic of the trapping properties of the devices containing magnetic particles compared with the reference group. The top friction layer caused charge flow, which produced a surface charge owing to contact. Owing to the characteristics of magnetic particles and dielectric polymers, the particles can act as a trapping site for free electrons and generate dipoles near themselves. This increased the surface-charge density and the flow of electrons through the external circuit, thereby enhancing the electrical-output characteristics.

Figure 3 depicts the trapping role played by the magnetic dots in the TENG structure in more detail. The TENG models

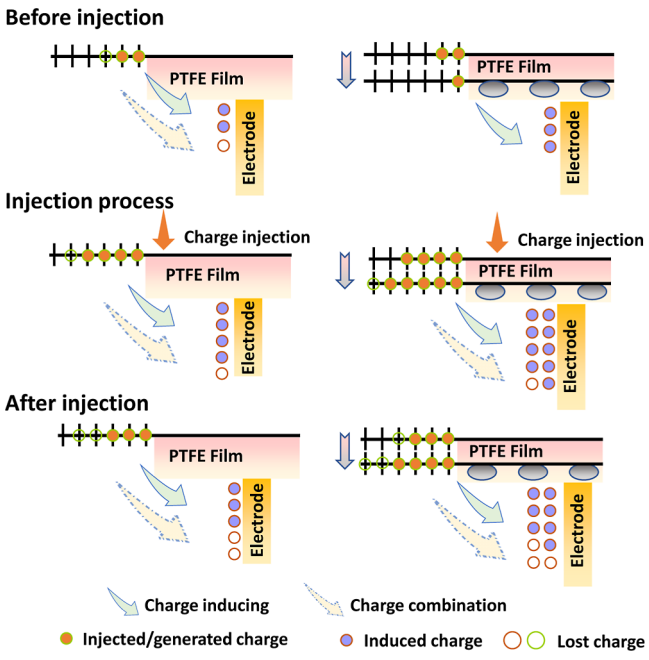

Figure 3. Charge transport and trapping mechanisms with/without magnetic particles.

with and without magnetic particles were further explained to describe the practical effect of the trapping properties on the voltage output. When the friction layers were in contact with each other, the surface charge generated by the contact process induced an opposite charge on the bottom electrode. In addition to the natural dissipation of charge in air, the back-electrode-induced charge also decreased the surface-charge density. When magnetic particles provide trapping sites, they effectively capture free electrons and prevent them from binding to the induced charge on the electrode, thereby preventing charge loss. In the process of charge injection, the magnetic particles acting as trapping sites can effectively capture the injected charge compared to the reference group without a trapping layer. Increasing the amount of captured charge can directly increase the surface-charge density and prevent it from combining with the charge on the electrode to avoid charge loss. After injection, the charge will inevitably dissipate into the air, resulting in loss. In this process, the surface charge continues to combine with the induced charge at the bottom electrode; thus, the charge level almost returns to its original level before injection after a few hours, resulting in a low output voltage. Because samples containing trapping sites effectively capture charges, they can slow the dissipation of charges to the air to a certain extent and block the combination of the surface and induced charges on the back electrode, thereby maintaining a high-voltage output after a few hours.[24]

Figure 4a shows the output voltage of the nylon dielectric layer coated with magnetic particles at the bottom (NM-P group); i shows the N-P group, and ii, iii, and iv show the 4 × 4, 6 × 6, and 8 × 8 dots of the NM-P groups, respectively (the output voltages of the TENG under different injection conditions are shown in Figures S4−S6 for 4 × 4, 6 × 6, and 8 × 8 dots, respectively). Notably, as shown in Figure 1c, nylon itself has brittle mechanical properties, and when relatively hard magnetic particles are added to the back side, the part close to the particles will incur damage during friction, thereby affecting the overall output voltage. In addition, nylon has poor trapping properties, and previous studies have indicated that the surface-charging performance of nylon after charge injection is worse than that of PTFE.[25] After injecting a voltage of +7 kV, little difference was observed between the 4 × 4 dot combination, 6 × 6 dot group, and the reference group, while the 8 × 8 dot group showed the lowest output voltage. This may be because the increase in the overall particle number inevitably caused air to fill the space between the friction layer and the electrode on the back, and the breakdown effect reduced the overall dielectric constant and capacitance level.[26] In addition, the excessive increase in the overall thickness of the TENG is a factor that cannot be ignored. As mentioned, an excessively strong magnetic field leads to the penetration of the electric field, which has a more adverse effect on the voltage output.[27,28] However, after undergoing charge injection, the three groups of samples containing magnetic particles showed better trapping properties than the reference group in 4000 friction cycles and retained a high-output state for a relatively long time. However, even with the addition of magnetic particles, the injection charge on the nylon surface could not maintain a high output state for a long time, and the 8 × 8 dots group showed the best trapping performance of 63% after 5000 friction cycles (63 V decayed to 40 V).

The next measurement was of the NM-PM structure, as shown in Figure 5a; i shows the N-P group, and ii, iii, and iv show the 4 × 4, 6 × 6, and 8 × 8 dots of the NM-PM groups, respectively. In this experiment, charge injections of +7 and −7 kV were performed on the surfaces of the positive and negative friction layers, respectively, and the friction experiment was conducted for 5000 consecutive cycles. The results showed that the output performance of the reference group without magnetic particles was superior. This result can be attributed to the obvious disadvantage of this structure: the positive and negative friction layers contain magnetic particle droplets

https://doi.org/10.1021/acsomega.3c07460
ACS Omega 2024, 9, 3565−3573

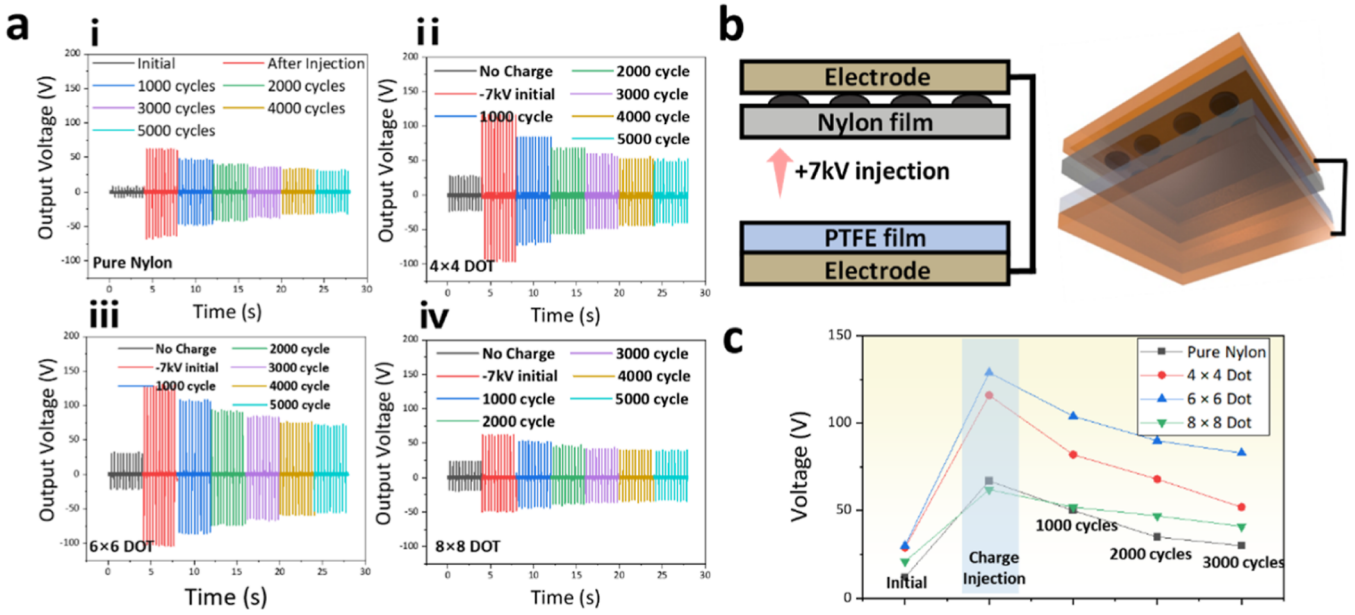

Figure 4. (a) Output measurement data of the (i) N-P and (ii–iv) NM-P TENG. (measured by cycles). (b) Schematic of the nylon–magnetic dot–electrode TENG. (c) The summary graph of the 4 samples is to compare the output performance.

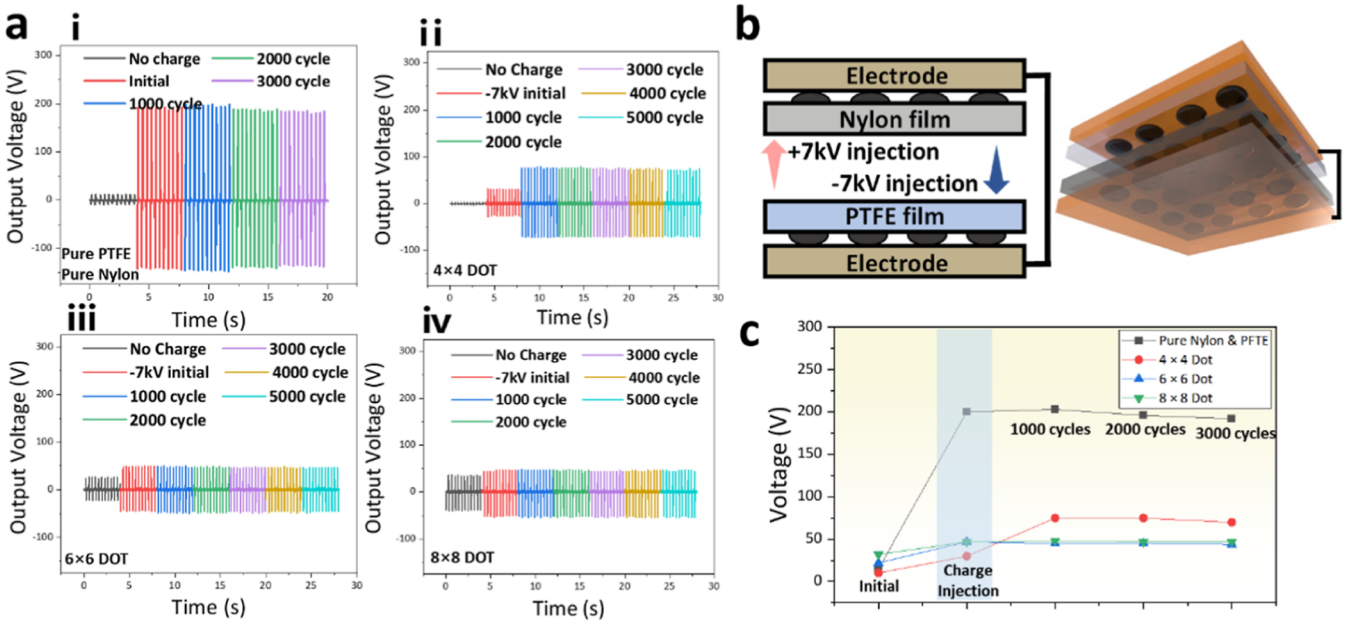

Figure 5. (a) Measurement data of the (i) N-P and (ii–iv) NM-PM TENG. (measured by cycles). (b) Schematic of the NM-PM TENG. (c) Summary graph of the 4 samples to compare the output performance.

simultaneously, and this part has an extra height. In this case, only the raised part of the magnetic particle droplets will experience friction, where the contact area changed to magnetic particle droplets, magnetic particle droplets from magnetic particle droplets opposite film, greatly reducing the friction contact area; also when the magnetic particle droplets are added on both sides at the same time, the thickness of the overall TENG will inevitably increase, which will also adversely affect the output voltage. However, its output performance continued to decline by approximately 10% (from 201 to 179 V) after 4000 cycles of friction. As more particles were introduced, the trapping property exhibited an increasing trend, and the output voltage of the 8 × 8 dot group was almost the same (reduced from −54 to −53 V) after the same 5000 cycles of friction. Although the overall output voltages of all groups with trapping layers were lower than those of the reference group, an increase in the trapping properties could be verified.

Finally, the N-PM structure was analyzed; Figure 6(i) shows the N-P group, and ii, iii, and iv show the 4 × 4, 6 × 6, and 8 × 8 dots of the N-PM groups, respectively. According to previous studies, PTFE has good trapping properties and can maintain a high surface charge for a certain period without the addition of trapping layers. The test results showed that when compared to the reference group, the output voltage increased but later declined as the number of magnetic particles increased. We estimated that the reason for the decrease in the output voltage in the 8 × 8 dot group was the same as that in the NM-P

https://doi.org/10.1021/acsomega.3c07460
ACS Omega 2024, 9, 3565−3573

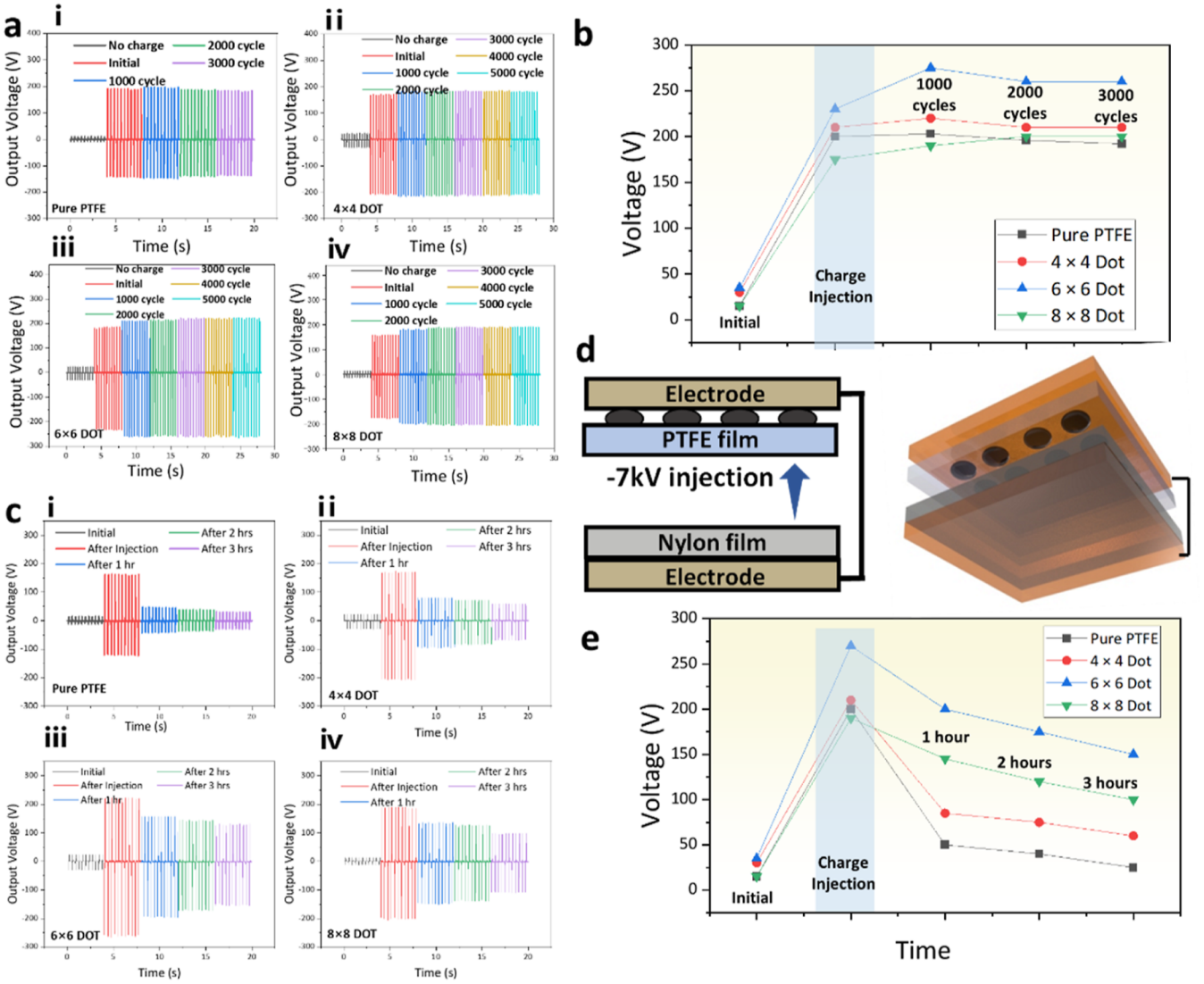

Figure 6. (a) Measurement data of the (i) N-P and (ii–iv) N-PM TENG (measured by cycles). (b) Summary graph of the 4 samples to compare the output performance. (c) Measurement data of the (i) N-P and (ii–iv) N-PM TENG (measured by hours). (d) Schematic of the N-PM TENG. (e) Summary graph of the 4 samples to compare the output performance (measured by hours).

group. As shown in Figure 6a,b, the 4 × 4 dot group demonstrated a high output voltage of 280 V after charge injection, 1.4 times that of the reference group of 200 V. Additionally, it maintained nearly the same output voltage after 5000 friction cycles, demonstrating high output performance over a long period. Figure 6c,e shows the voltage test results measured once every hour without continuous friction. The reason for applying this measurement is that in a state of continuous friction, new surface charges are constantly generated owing to electrostatic-induction effects; therefore, observing the phenomenon of charge decay is difficult [as shown in Figure 6a(i), even after 4000 cycles of friction, the charge is only reduced by 10%]. To better observe the charge-decay phenomenon, the test time was set to once every hour. The test results showed that the output voltage of the sample without a trapping layer rapidly decreased by 75% (from 164 to 46 V) after 1 h of injection and almost decreased to its original value before injection after 3 h of injection (28 V). With an increase in the number of magnetic particles, the trapping properties improved. After 3 h of injection, the 4 × 4, 6 × 6, and 8 × 8 dots maintained outputs of 33% (207 to 69 V), 59% (259 to 153 V), and 58% (193 to 112 V) of the highest output voltage after charge injection, respectively. In addition, the output voltage 3 h after the injection process showed that the N-PM 6 × 6 dot group maintained a considerably higher output level (153 V) than that of the reference N-P group (28 V). This realized the goal of maintaining a high output for a long time.

Figure 7 shows the performance and practical applications of the TENG device after the charge injection. Figure 7a shows a circuit diagram of the TENG when load resistance was applied for testing. The output voltage and current were measured using changes in applied resistance to calculate the actual output power of the TENG. As shown in Figure 7b, after the charge injection, the output voltage gradually increased from 12 to 220 V with an increase in resistance, whereas the output current decreased from 2.8 to 0.1 mA. The actual output power of the entire TENG reached its highest value of 167 mW/m^2 at 2×10^{-7} Ω. As part of the practical application, we chose a sample of the N-PM structure and first performed charge injection. Figure 7d shows the sensitivity of the TENG as a sensor. By applying different forces, holding them for

https://doi.org/10.1021/acsomega.3c07460
ACS Omega 2024, 9, 3565−3573

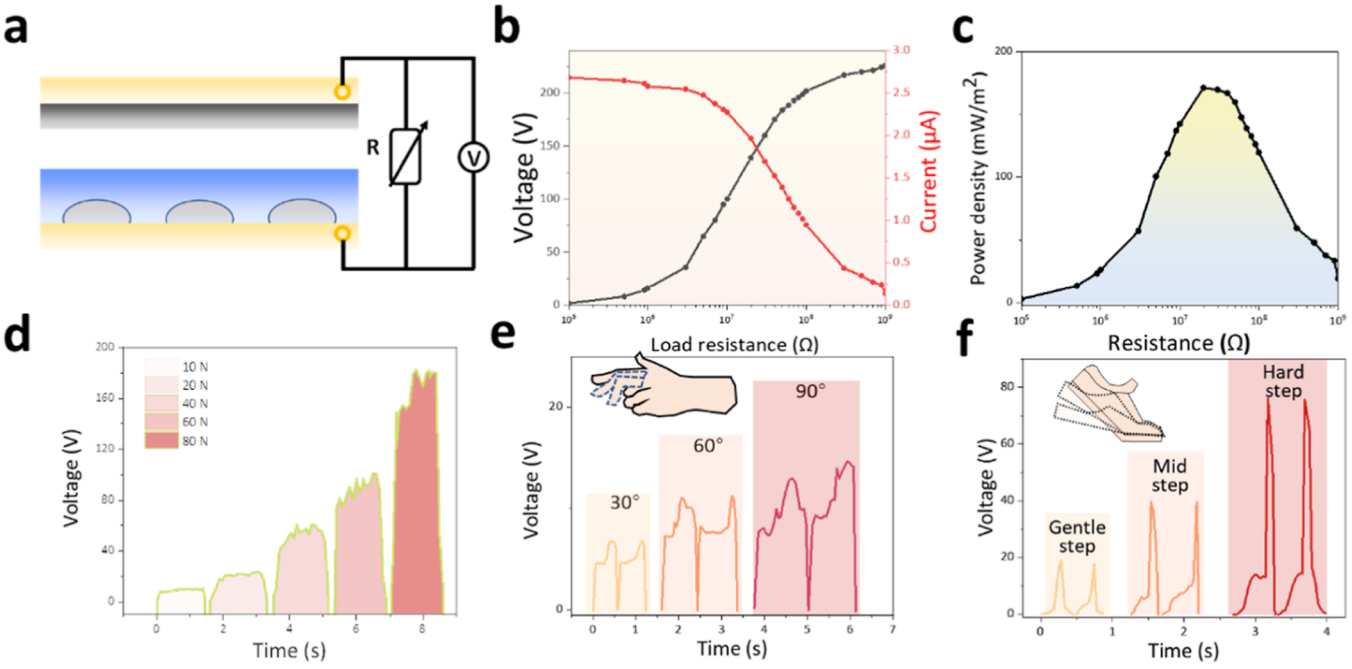

Figure 7. (a) Schematic of the circuit of the load resistance measurement. (b) Voltage and current changes depend on the load resistance. (c) Power calculated by the load resistance measurement. (d) Sensitivity measurement under different pressure. (e) Performance of the wrist bending sensor. (f) Performance of step sensor.

approximately 1 s, and releasing them again, the measurement results showed that the sensor maintained the same proportional growth when the stress increased, indicating good sensitivity. Figure 7e,f shows the performance of the sensor when strapped to the wrist of a person and placed under the insole, respectively. With an increase in the degree of wrist bending, the output voltage showed a gradually increasing trend, and the shape of the output signal was maintained, showing a stable sensing performance. When the sensor was pressed under the insole with different actions, such as "gentle step, mid step, and hard step", the frequency and size of the signal changed correspondingly, which confirmed the good sensitivity of the sensor. (The photograph of the finger bending sensor and the insole walking sensor is shown in Figures S7 and S8. The video of the finger bending sensor is shown in Video S1.)

CONCLUSIONS

In summary, elastomer ink droplets containing magnetic nickel were coated on the back of the dielectric layer of PTFE and the nylon films. The magnetic substances in the elastomer were used as trapping sites to maintain the surface charge caused by charge injection and to prevent the combination of induced and friction layer charges. Thus, the maximum surface-charge density was preserved for a longer period and the output voltage increased. The number of magnetic particles and the N-PM, NM-P, and NM-PM structures were compared as variables. After the charge-injection process, compared with the basic control group N-P, the N-PM group exhibited a higher output voltage (260 V) after 4000 cycles of friction and showed no downward trend, maintaining 59% (259 to 153 V) of the voltage just after injection and even after 3 h of rest, which was more than 5.5 times that of the reference group (28 V). The results prove that the particles in magnetic ink provide trapping properties and effectively maintain the high charge level caused by charge injection over a long time. The TENG was used as a general sensor to detect different movement behaviors of the human body, thereby proving its practical-application significance.

ASSOCIATED CONTENT

Data Availability Statement

The data that support the findings of this study are available in the Supporting Information of this article.

Supporting Information

The Supporting Information is available free of charge at https://pubs.acs.org/doi/10.1021/acsomega.3c07460.

SEM images showing the nickle particles distribution, photographs of the push−pull gauge and the charge injection device, the output measurement of 4 × 4, 6 × 6, 8 × 8 dot coated TENG, the photograph of finger bending sensor and the insole sensor (PDF)

The video of finger bending sensor (AVI)

AUTHOR INFORMATION

Corresponding Authors

Jong-Jin Park − *Department of Polymer Science and Engineering, Chonnam National University, Gwangju 61186, Republic of Korea;* orcid.org/0000-0002-8386-3594; Email: jjpark@jnu.ac.kr

Jihyun Bae − *Human-Tech Convergence Program, Department of Clothing & Textiles, Hanyang University, Seoul 04763, Republic of Korea;* orcid.org/0000-0003-2143-6308; Email: jbae2@hanyang.ac.kr

Authors

Jingzhe Sun − *Human-Tech Convergence Program, Department of Clothing & Textiles, Hanyang University, Seoul 04763, Republic of Korea; Department of Polymer Science and Engineering, Chonnam National University,*

https://doi.org/10.1021/acsomega.3c07460
ACS Omega 2024, 9, 3565−3573

Gwangju 61186, Republic of Korea; orcid.org/0000-0003-3573-4306

Jiwoo Lee − *Department of Polymer Science and Engineering, Chonnam National University, Gwangju 61186, Republic of Korea*

Seunghye Han − *Department of Polymer Science and Engineering, Chonnam National University, Gwangju 61186, Republic of Korea*

Yongwei Li − *Human-Tech Convergence Program, Department of Clothing & Textiles, Hanyang University, Seoul 04763, Republic of Korea*

Complete contact information is available at: https://pubs.acs.org/10.1021/acsomega.3c07460

Author Contributions

[§]J.S. and J.L. contributed equally to this work.

Notes

The authors declare no competing financial interest.

■ ACKNOWLEDGMENTS

This work is supported by the Basic Science Research Program through the National Research Foundation of Korea (NRF) funded by the Ministry of Education (NRF-2022R1A2C2010760). This result was supported by "Regional Innovation Strategy (RIS)" through the National Research Foundation of Korea (NRF) funded by the Ministry of Education (MOE) (2021RIS-002).

■ REFERENCES

(1) Tarhan, C.; Çil, M. A. A Study on Hydrogen, the Clean Energy of the Future: Hydrogen Storage Methods. *J. Energy Storage* **2021**, *40*, 102676.

(2) Jaiswal, K. K.; Chowdhury, C. R.; Yadav, D.; Verma, R.; Dutta, S.; Jaiswal, K. S.; SangmeshB; Karuppasamy, K. S. K. Renewable and Sustainable Clean Energy Development and Impact on Social, Economic, and Environmental Health. *Energy Nexus* **2022**, *7*, 100118.

(3) Hassan, A.; Ilyas, S. Z.; Jalil, A.; Ullah, Z. Monetization of the Environmental Damage Caused by Fossil Fuels. *Environ. Sci. Pollut. Res.* **2021**, *28* (17), 21204−21211.

(4) Wang, C.; Wang, P.; Chen, J.; Zhu, L.; Zhang, D.; Wan, Y.; Ai, S. Self-Powered Biosensing System Driven by Triboelectric Nanogenerator for Specific Detection of Gram-Positive Bacteria. *Nano Energy* **2022**, *93*, 106828.

(5) Dong, K.; Peng, X.; Wang, Z. L. Fiber/Fabric-Based Piezoelectric and Triboelectric Nanogenerators for Flexible/Stretchable and Wearable Electronics and Artificial Intelligence. *Adv. Mater.* **2019**, *32*, 1902549.

(6) Xie, Y.; Ma, Q.; Yue, B.; Chen, X.; Jin, Y.; Qi, H.; Hu, Y.; Yu, W.; Dong, X.; Jiang, H. Triboelectric Nanogenerator Based on Flexible Janus Nanofiber Membrane with Simultaneous High Charge Generation and Charge Capturing Abilities. *Chem. Eng. J.* **2023**, *452*, 139393.

(7) Kim, J.; Ryu, H.; Lee, J. H.; Khan, U.; Kwak, S. S.; Yoon, H.; Kim, S. High Permittivity $CaCu_3Ti_4O_{12}$ Particle-Induced Internal Polarization Amplification for High Performance Triboelectric Nanogenerators. *Adv. Energy Mater.* **2020**, *10* (9), 1903524.

(8) Yoon, H.-J.; Kim, D.-H.; Seung, W.; Khan, U.; Kim, T. Y.; Kim, T.; Kim, S.-W. 3D-Printed Biomimetic-Villus Structure with Maximized Surface Area for Triboelectric Nanogenerator and Dust Filter. *Nano Energy* **2019**, *63*, 103857.

(9) Bai, Y.; Xu, L.; Lin, S.; Luo, J.; Qin, H.; Han, K.; Wang, Z. L. Charge Pumping Strategy for Rotation and Sliding Type Triboelectric Nanogenerators. *Adv. Energy Mater.* **2020**, *10* (21), 2000605.

(10) Xu, L.; Bu, T. Z.; Yang, X. D.; Zhang, C.; Wang, Z. L. Ultrahigh Charge Density Realized by Charge Pumping at Ambient Conditions for Triboelectric Nanogenerators. *Nano Energy* **2018**, *49*, 625−633.

(11) Kim, D. W.; Lee, J. H.; You, I.; Kim, J. K.; Jeong, U. Adding a Stretchable Deep-Trap Interlayer for High-Performance Stretchable Triboelectric Nanogenerators. *Nano Energy* **2018**, *50*, 192−200.

(12) Jiang, H.; Lei, H.; Wen, Z.; Shi, J.; Bao, D.; Chen, C.; Jiang, J.; Guan, Q.; Sun, X.; Lee, S.-T. Charge-Trapping-Blocking Layer for Enhanced Triboelectric Nanogenerators. *Nano Energy* **2020**, *75*, 105011.

(13) Wu, C.; Kim, T. W.; Park, J. H.; An, H.; Shao, J.; Chen, X.; Wang, Z. L. Enhanced Triboelectric Nanogenerators Based on MoS_2 Monolayer Nanocomposites Acting as Electron-Acceptor Layers. *ACS Nano* **2017**, *11* (8), 8356−8363.

(14) Li, Z.; Zhu, M.; Qiu, Q.; Yu, J.; Ding, B. Multilayered Fiber-Based Triboelectric Nanogenerator with High Performance for Biomechanical Energy Harvesting. *Nano Energy* **2018**, *53*, 726−733.

(15) Seol, M. L.; Han, J. W.; Moon, D. I.; Yoon, K. J.; Hwang, C. S.; Meyyappan, M. All-Printed Triboelectric Nanogenerator. *Nano Energy* **2018**, *44* (November 2017), 82−88.

(16) Huang, L.; Xu, W.; Bai, G.; Wong, M.-C.; Yang, Z.; Hao, J. Wind Energy and Blue Energy Harvesting Based on Magnetic-Assisted Noncontact Triboelectric Nanogenerator. *Nano Energy* **2016**, *30*, 36−42.

(17) Xu, W.; Huang, L.-B.; Hao, J. Fully Self-Healing and Shape-Tailorable Triboelectric Nanogenerators Based on Healable Polymer and Magnetic-Assisted Electrode. *Nano Energy* **2017**, *40*, 399−407.

(18) Seol, M. L.; Han, J. W.; Moon, D. I.; Meyyappan, M. Hysteretic Behavior of Contact Force Response in Triboelectric Nanogenerator. *Nano Energy* **2017**, *32* (December 2016), 408−413.

(19) Sun, R.; Gao, L.; Shou, M.; Li, B.; Chen, X.; Wang, F.; Mu, X.; Xie, L.; Liao, C. Tribo-Material Based on a Magnetic Polymeric Composite for Enhancing the Performance of Triboelectric Nanogenerator. *Nano Energy* **2020**, *78*, 105402.

(20) Choong, C.-L.; Shim, M.-B.; Lee, B.-S.; Jeon, S.; Ko, D.-S.; Kang, T.-H.; Bae, J.; Lee, S. H.; Byun, K.-E.; Im, J.; Jeong, Y. J.; Park, C. E.; Park, J.-J.; Chung, U.-In. Highly Stretchable Resistive Pressure Sensors Using a Conductive Elastomeric Composite on a Micropyramid Array. *Adv. Mater.* **2014**, *26* (21), 3451−3458.

(21) Wang, S.; Xie, Y.; Niu, S.; Lin, L.; Liu, C.; Zhou, Y. S.; Wang, Z. L. Maximum Surface Charge Density for Triboelectric Nanogenerators Achieved by Ionized-Air Injection: Methodology and Theoretical Understanding. *Adv. Mater.* **2014**, *26* (39), 6720−6728.

(22) Sun, J.; Ren, B.; Han, S.; Shin, H.; Cha, S.; Lee, J.; Bae, J.; Park, J. Amplified Performance of Charge Accumulation and Trapping Induced by Enhancing the Dielectric Constant via the Cyano Group of 3D-Structured Textile for a Triboelectric Multi-Modal Sensor. *Small Methods* **2023**, *7*, 2300344.

(23) Tang, Y.; Xu, B.; Gao, Y.; Li, Z.; Tan, D.; Li, M.; Liu, Y.; Huang, J. Ultrastrong-Polar Polyacrylonitrile Organic-Inorganic Architected Nanogenerators with Synergistic Triboelectric Behavior for Efficient Biomechanical Energy Harvesting and Self-Powered Sensing. *Nano Energy* **2022**, *103*, 107833.

(24) Yi, H.; Xiong, L. The Effect of the Electric Field on the Output Performance of Triboelectric Nanogenerators. *J. Comput. Electron.* **2020**, *19* (4), 1670−1677.

(25) Cha, S.; Cho, Y.; Kim, J. G.; Choi, H.; Ahn, D.; Sun, J.; Kang, D.; Pak, C.; Park, J. Controllable Triboelectric Series Using Gradient Positive and Negative Charge-Confinement Layer with Different Particle Sizes of Mesoporous Carbon Materials. *Small Methods* **2022**, *6* (5), 2101545.

(26) Zi, Y.; Wu, C.; Ding, W.; Wang, Z. L. Maximized Effective Energy Output of Contact-Separation-Triggered Triboelectric Nanogenerators as Limited by Air Breakdown. *Adv. Funct. Mater.* **2017**, *27* (24), 1700049.

(27) Vu, D.-L.; Ahn, K.-K. Triboelectric Enhancement of Polyvinylidene Fluoride Membrane Using Magnetic Nanoparticle for Water-Based Energy Harvesting. *Polymers* **2022**, *14* (8), 1547.

(28) Chakraborty, I.; Lai, S.-N.; Wu, M.-C.; Lin, H.-Y.; Li, C.; Wu, J. M.; Lai, C.-S. Charge Trapping with α-Fe_2O_3 Nanoparticles Accompanied by Human Hair towards an Enriched Triboelectric Series and a Sustainable Circular Bioeconomy. *Mater. Horiz.* **2021**, *8* (11), 3149−3162.

https://doi.org/10.1021/acsomega.3c07460
ACS Omega 2024, 9, 3565−3573